On the origins of temporal power-law behavior in the global atmospheric circulation

Dmitry I. Vyushin, Paul J. Kushner, Josh Mayer

Department of Physics, University of Toronto, Toronto, Ontario, Canada

D. I. Vyushin, Department of Physics, University of Toronto, 60 St. George Str., Toronto, Ontario, M5S 1A7, Canada. (dmitry.vyushin@utoronto.ca)

Climate variations on timescales longer than a year are often characterized by temporal scaling (“power-law”) behavior for which spectral power builds up at low frequencies in contrast to red-noise behavior for which spectral power saturates at low frequencies. Checks on the ability of climate prediction models to simulate temporal scaling behavior represent stringent performance tests on the models. We here estimate temporal power-law exponents (“Hurst exponents”) for the global atmospheric circulation of the stratosphere and troposphere during the 20th century. We show that current-generation climate models generally simulate the spatial distribution of the Hurst exponents well. We then use simulations with different climate forcings to explain the Hurst exponent distribution and to account for discrepancies in scaling behavior between different observational products. We conclude that characterization of temporal power-law behavior provides a valuable tool for cross-validating low-frequency variability in various datasets, for elucidating the physical mechanisms underlying this variability, and for statistical testing of trends and periodicities in climate time series.

1. Introduction

Climate variability on interannual to multi-decadal time scales involves a mix of externally and internally generated variability [*Wigley and Raper*, 1990]. The classical two-parameter model of such variability is *Hasselmann* [1975] autoregressive model of the first order (AR1). It corresponds to a class of physical models in which stochastic (weather-noise) atmospheric variability drives slower components of the climate system such as the ocean. An alternative two-parameter model of the temporal power spectrum is the power-law model

$$S_{PL}(\lambda) = b|\lambda|^{1-2H}, \quad 0 < \lambda_l \leq |\lambda| \leq \lambda_h \leq 1/2, \tag{1}$$

where λ is the frequency, b represents the overall spectral power, the "Hurst exponent" H is related to the spectral slope s by $H = (1-s)/2$, and λ_l and λ_h are low and high frequency cutoffs used in model fitting. Unlike the Hasselmann model, the power-law model, which indicates temporal scaling behavior rather than dependence on any particular timescale, has no simple established physical interpretation.

Recent research has pointed out potential limitations of the AR1 model [e.g. *Hall and Manabe*, 1997] and has shown that power-law scaling behavior arises in surface air temperature [*Pelletier*, 2002; *Blender and Fraedrich*, 2003; *Huybers and Curry*, 2006], the atmospheric circulation [*Tsonis et al.*, 1999; *Vyushin and Kushner*, 2009], etc. The current instrumental record is too short to statistically claim the superiority of the one model over the other on timescales shorter than a century, but there are locations where power-law seems to fit the observations better than AR1 [*Percival et al.*, 2001; *Vyushin et al.*, 2007; *Vyushin and Kushner*, 2009]. We therefore do not claim that power-law behavior is universal on all timescales, and instead use $S_{PL}(\lambda)$ to provide a sense of how quickly power builds towards lower frequencies. Regions where $\hat{H} = 0.5$ (the flat spectrum limit) might be well described by either model, while regions where $\hat{H}$ is closer to 1 (the $1/f$ limit) are candidates for true power-law behavior.

We here report on how climate prediction models can be used to simulate and explain the observed spatial distribution of the Hurst exponent estimate $\hat{H}$ for the atmospheric general circulation. To do so, we compare $\hat{H}$ from observationally based reanalysis products to comprehensive climate simulations, and then use more specialized simulations to explain specific features of the $\hat{H}$ field. Previous model-observation comparisons have concluded that the ability of climate models to simulate the observed scaling is mixed [*Govindan et al.*, 2002; *Blender and Fraedrich*, 2003; *Vyushin et al.*, 2004], but this work has generally been restricted to surface air temperature and has proven to be method and model dependent. We here carry out physically motivated analyses and provide cross-validation checks that are independent of the Hurst exponent estimation technique. In separate work, we have verified that alternative Hurst exponent methods provide similar results [*Vyushin and Kushner*, 2009].

2. Data and Methods

To estimate H for $S_{PL}(\lambda)$ in (1), we use detrended fluctuation analysis of the third order [DFA3, *Kantelhardt et al.*, 2001]. See the supplementary information for DFA3 details and a comparison of its results to another method. We estimate H for the zonal-mean air temperature data in the range of 18 months to 45 years for the NCEP/NCAR and ERA40 reanalyses for the period 09.1957-08.2002. We compare these estimates to several model simulations: simulations of the GFDL AM2.1-LM2.1 atmospheric general circulation model [*The GFDL Global Atmospheric Model Development Team*, 2004], for which sea surface temperatures (SSTs) are prescribed, and 17 coupled model runs of the 20th century from the CMIP3 archive. All model simulations were taken for the period 01.1955-12.1999. Additional model details are provided in the supplementary information. Because the quasi-biennial oscillation (QBO) is not captured by any of the models considered, we filter the QBO signal from the reanalyses temperature in addition to the seasonal cycle [*Vyushin et al.*, 2007].

3. Results and Discussion

Fig. 1 plots estimates of H for the reanalysis products and several climate simulations. The $\hat{H}$ distribution displays a characteristic shape that we have verified is robust to different methods of H estimation [*Vyushin and Kushner*, 2009]. Both the NCEP/NCAR and ERA40 reanalyses (Figs. 1a and b) show maxima in $\hat{H}$ in the tropical to low-extratropical troposphere and in the tropical to subtropical stratosphere and a minimum in the Northern Hemisphere polar stratosphere. But there are differences between the reanalysis products; for example, ERA40 has separate local maxima in $\hat{H}$ in the lower and upper troposphere at 60^0S that will be discussed later in relation to Fig. 3. We will also show that even where the distributions appear to agree, they might do so for different reasons.

Fig. 1c plots the $\hat{H}$ distribution for a simulation of AM2.1 forced by historical SSTs, anthropogenic greenhouse gases and aerosols, ozone changes, solar flux, and volcanic aerosols (hereafter the “HistSST+AllForc” simulation). The main features of the $\hat{H}$ distribution of this simulation are similar to that displayed in the observationally based Figs. 1a-b, including the falloff of $\hat{H}$ as we move from the equator to the poles and separate maxima in the lower stratosphere and the troposphere. Therefore given historical SSTs and the other principal external forcings GFDL AM2.1 is able to reproduce the continuum of zonal mean temperature variability represented by the Hurst exponent.

We use three additional simulations of AM2.1 to explain the $\hat{H}$ distribution: 1) "Climo", a simulation in which the climate forcings including SSTs are not allowed to vary from year to year. The "Climo" simulation has $\hat{H}$ values fairly close to 0.5 everywhere, with a range of between 0.4 and 0.6 (not shown). This supports Hasselmann's assumption of a flattening out of the spectrum at low frequencies, demonstrating an absence of long-term memory in the atmosphere in the absence of coupling to the ocean; 2) "HistSST", a simulation that is forced with historical SSTs but that keeps all other climate forcings fixed. The "HistSST" simulation (Fig. 1d) gives rise to a tropospheric pattern of $\hat{H}$ that is similar to that in Figs. 1a-c. This is consistent with our classical understanding that the tropospheric circulation and thermal structure are largely determined once the SSTs are prescribed on timescales longer than the atmospheric adjustment timescale of a few months; 3) "Vol", a simulation that is forced with the "Climo" SSTs but that uses historical volcanic forcing, while keeping all other forcings fixed. The "Vol" simulation (Fig. 1e) gives rise to a stratospheric pattern of $\hat{H}$ that is similar to that in Figs. 1a-c. Thus, the simulations show that the observed $\hat{H}$ distribution is mainly determined by temporal variability of the SSTs in the troposphere and by volcanic forcing in the lower stratosphere.

We briefly demonstrate that current generation climate models can capture the $\hat{H}$ distribution in a less constrained forcing framework. The $\hat{H}$ distribution averaged over the CMIP3 coupled ocean-atmosphere models is shown in Fig. 1f; it displays a similar structure to Figs. 1a-c but has a narrower meridional extent and a weaker volcanic signature in the lower stratosphere. The simple explanation for the latter is that only 9 of the 17 models considered included realistic volcanic forcings.

We propose that the relatively steep spectral slopes represented by the $\hat{H}$ maximum centered in the tropical troposphere are generated by tropical SST variability. Our test of this idea reveals a significant discrepancy between the two reanalysis products. To test the idea, we create time series of tropical mean SST in the latitude band 20^0S-20^0N ("TropSST"). We then filter the TropSST signal from the temperature time series and estimate H of the result for the NCEP/NCAR and ERA40 reanalyses and for the HistSST+AllForc simulations. Fig. 2 isolates the part of the $\hat{H}$ distribution related to tropical SSTs by showing the original $\hat{H}$ minus the TropSST-filtered $\hat{H}$. In the NCEP/NCAR reanalysis (Fig. 2a) and in the simulation (Fig. 2c), there is a vertically coherent part of the $\hat{H}$ distribution throughout the tropical and low extratropical troposphere that is related to the TropSST signal, as indicated by the positive values. The TropSST $\hat{H}$ signature in the ERA40 reanalysis (Fig. 2b) is qualitatively different, being vertically incoherent and of mixed sign.

In Fig. 2, the NCEP/NCAR reanalysis and the climate model simulation appear to agree with our hypothesis of tropical SST control, while the ERA40 appears to disagree with it. To understand these inconsistent results we display the residuals of the tropical upper tropospheric temperatures after TropSST filtering has been applied, for the reanalysis products and for the HistSST+AllForc and HistSST simulations (Fig. 3a). A one year running average has also been applied. The ERA40 residuals (shown in red) show much more decadal variance than the NCEP/NCAR residuals and the simulations' residuals. Significant fluctuations for the ERA40 include particularly high values during 1975-1983, which are probably related to problems with transition from VTPR to TOVS satellite data [*Simmons et al.*, 2004; *Uppala and Coauthors*, 2005], and low values after 1992. Similar issues also explain the lower and upper tropospheric $\hat{H}$ maxima at 60^0S that are seen in the ERA40 reanalysis (Fig. 1b) but not seen in the NCEP/NCAR reanalysis (Fig. 1a) or in the HistSST+AllForc simulation (Fig. 1c). Figs. 3b and c plot temperature anomalies (without TropSST filtering) from the same four data sets at these locations. There is an obvious jump (negative at 925hPa and positive at 300hPa) in the ERA40 temperature presumably related to problems with assimilation of the VTPR data from 1973 to 1978 [*Bengtsson et al.*, 2004; *Simmons et al.*, 2004]. Another striking difference between the models and reanalyses are the strong positive trends at 300hPa. These trends seem to be spurious and stem from the reanalysis models cold biases combined with a gradual increase in the amount of observations in the Southern Hemisphere [*Bengtsson et al.*, 2004; *Simmons et al.*, 2004]. Discrepancies in the Southern Hemisphere polar stratosphere have been discussed elsewhere [*Vyushin and Kushner*, 2009]. Therefore data inhomogeneity issues in the ERA40 affect and are revealed by our H analysis.

4. Conclusions

To conclude, we find that zonal-mean air temperature on interannual to multi-decadal timescales has a steep spectrum that might be modelled by power-law behavior in the tropical to low-extratropical troposphere and the tropical to subtropical stratosphere. Current generation climate models can capture these features and specialized forcing simulations elucidate their dynamics. We propose that the tropospheric $\hat{H}$ signatures are linked to tropical SST variability and that the lower stratospheric $\hat{H}$ signatures are linked to volcanic forcing. The link to tropical SST variability is clear in only one of the two observational products we use: the NCEP/NCAR reanalysis. The large $\hat{H}$ values in the tropical upper troposphere in the ERA40 reanalysis appears to arise from data problems that mask the connection to tropical SSTs. The ERA40 H estimates also exhibits tropospheric maxima at 60^0S that appear related to other documented data assimilation issues.

This analysis points to problems in naively interpreting the Hurst exponent distribution as an indicator of long-term memory in climate and care needs to be taken to elucidate the physical basis for a given $\hat{H}$ feature. Data inhomogeneities affect many observational time series and can equally give rise to power-law behavior [*Berton*, 2004; *Rust et al.*, 2008]. Sometimes, such as at 60^0S in the troposphere, it is immediately evident that there is a discrepancy to explain, but at other times, such as in the tropical troposphere, the effort still needs to be made to test the consistency of the power-law behavior under different physical hypotheses. We have found that general circulation models provide a useful tool for such testing.

The frequent presence of power-law behavior, whatever its cause, suggests that statistical testing for significant trends and periodicities should use power-law noise models [*Smith*, 1993; *Vyushin et al.*, 2007] as well as AR1-models, particularly in the tropical upper troposphere and lower stratosphere where $\hat{H}$ is large and trend evaluation has proven difficult [e.g. *Santer et al.*, 2005]. Power-law based confidence intervals are typically larger because they assume more power at lower frequencies. For example, power-law based significance testing has been applied to the problem of stratospheric ozone recovery in the presence of significant stratospheric internal variability, and leads to a lengthening of the projected time for the detection of ozone recovery [*Vyushin et al.*, 2007].

References

Bengtsson, L., S. Hagemann, and K. I. Hodges (2004), Can climate trends be calculated from reanalysis data?, *J. Geophys. Res.*, *109*, D11,111, doi:10.1029/2004JD004536.

Berton, R. P. H. (2004), Influence of a discontinuity on the spectral and fractal analysis of one-dimensional data, *Nonlin. Processes Geophys.*, *11*, 659–682.

Blender, R., and K. Fraedrich (2003), Long time memory in global warming simulations, *Geophys. Res. Lett.*, doi:10.1029/2003GL017666.

Govindan, R. B., D. Vyushin, S. Brenner, A. Bunde, S. Havlin, and H.-J. Schellnhuber (2002), Global climate models violate scaling of the observed atmospheric variability, *Phys. Rev. Lett.*, *89*, 028,501.

Hall, A., and S. Manabe (1997), Can local linear stochastic theory explain sea surface temperature and salinity variability?, *Climate Dynamics*, *13*, 167–180, doi: 10.1007/s003820050158.

Hasselmann, K. (1975), Stochastic climate models, part 1: Theory, *Tellus*, *28*, 473–485.

Huybers, P., and W. Curry (2006), Links between annual, Milankovitch, and continuum temperature variability, *Nature*, *441*, doi:10.1038/nature04745.

Kantelhardt, J. W., E. Koscielny-Bunde, H. H. A. Rego, S. Havlin, and A. Bunde (2001), Detecting long-range correlations with detrended fluctuation analysis, *Physica A*, *295*, 441–454.

Pelletier, J. D. (2002), Natural variability of atmospheric temperatures and geomagnetic intensity over a wide range of time scales, *Proc. Natl. Acad. Sci. (USA)*, *99*, 2546–2553.

Percival, D. B., J. E. Overland, and H. O. Mofjeld (2001), Interpretation of North Pacific variability as a short- and long-memory process, *J. Climate*, *14*, 4545–4559.

Rust, H. W., O. Mestre, and V. K. C. Venema (2008), Fewer jumps, less memory: Homogenized temperature records and long memory, *J. Geophys. Res.*, *113*, D19,110, doi:10.1029/2008JD009919.

Santer, B. D., T. M. L. Wigley, C. Mears, F. J. Wentz, and S. A. Klein (2005), Amplification of surface temperature trends and variability in the tropical atmosphere, *Science*, *309*, 1551–1556, doi:10.1126/science.1114867.

Simmons, A. J., P. D. Jones, V. da Costa Bechtold, A. C. M. Beljaars, P. W. Kallberg, S. Saarinen, S. M. Uppala, P. Viterbo, and N. Wedi (2004), Comparison of trends and low-frequency variability in CRU, ERA-40 and NCEP/NCAR analyses of surface air temperature, *J. Geophys. Res.*, *109*, D24,115, doi:10.1029/2004JD005306.

Smith, R. L. (1993), Long-range dependence and global warming, in *Statistics for the Environment*, edited by V. Barnett and F. Turkman, pp. 141–161, John Wiley, Chichester.

The GFDL Global Atmospheric Model Development Team (2004), The new GFDL global atmosphere and land model AM2-LM2: Evaluation with prescribed SST simulations, *J. Climate*, *17*, 4641–4673.

Tsonis, A. A., P. J. Roebber, and J. B. Elsner (1999), Long-range correlations in the extratropical atmospheric circulation: origins and implications, *J. Climate*, *12*, 1534–1541.

Uppala, and Coauthors (2005), The ERA-40 re-analysis, *Quart. J. Roy. Meteor. Soc.*, *131*, 2961–3012, doi:10.1256/qj.04.176.

Vyushin, D. I., and P. J. Kushner (2009), Power-law and long-memory characteristics of the atmospheric general circulation, *J. Climate (in press)*.

Vyushin, D. I., I. Zhidkov, S. Havlin, A. Bunde, and S. Brenner (2004), Volcanic forcing improves Atmosphere-Ocean Coupled General Circulation Model scaling performance, *Geophys. Res. Lett.*, *31*, doi:10.1029/2004GL019499.

Vyushin, D. I., V. E. Fioletov, and T. G. Shepherd (2007), Impact of long-range correlations on trend detection in total ozone, *J. Geophys. Res.*, *112*, doi: 10.1029/2006JD008168.

Wigley, T. M. L., and S. C. B. Raper (1990), Natural variability of the climate system and detection of the greenhouse effect, *Nature*, *344*, 324–327, doi:10.1038/344324a0.

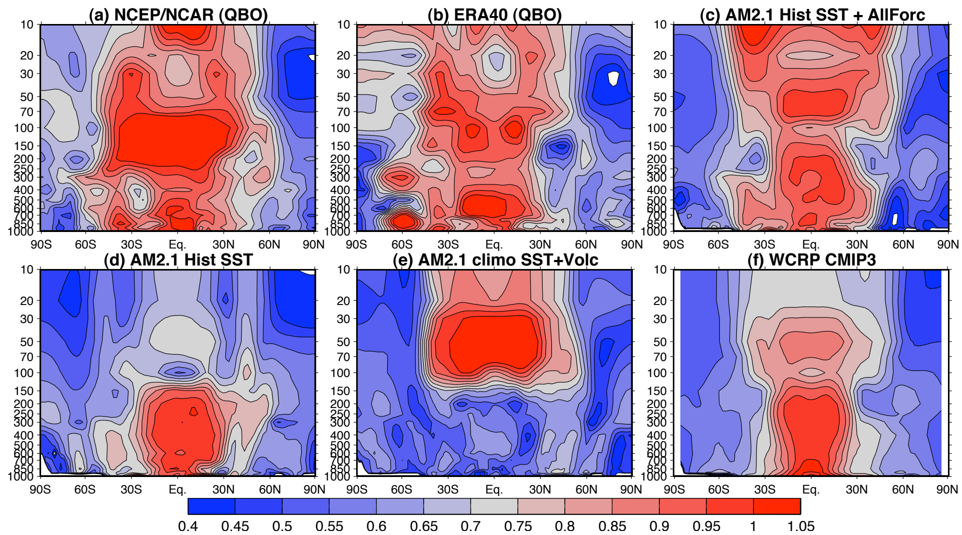

Figure 1. $\hat{H}$ distribution for zonal-mean temperature for (a) the NCEP/NCAR reanalysis, (b) the ERA40 reanalysis, (c) the GFDL AM2.1 HistSST+AllForc simulation, (d) the GFDL AM2.1 HistSST simulation, (e) the GFDL AM2.1 Vol simulation, (f) the CMIP3 simulations. Panel (f) represents a multiple model average. As stated in the text, QBO filtering has been applied to the reanalysis temperatures in Figs. 1a-b.

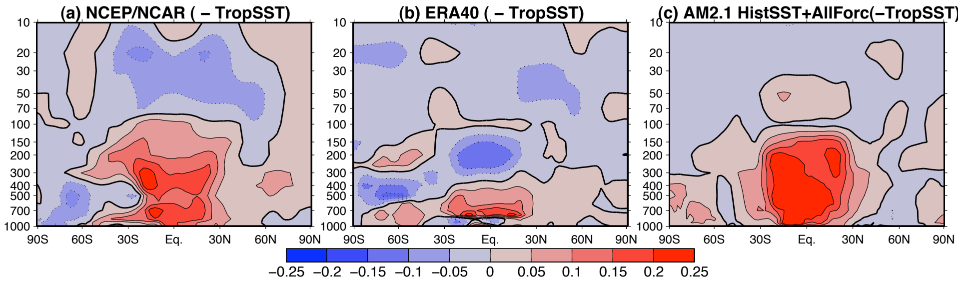

Figure 2. $\hat{H}$ without TropSST filtering minus $\hat{H}$ with TropSST filtering, which represents the signature of the tropical SSTs in the $\hat{H}$ field: (a) NCEP/NCAR, (b) ERA40, (c) AM2.1 HistSST+AllForc. QBO filtering has been applied to ERA40 and NCEP/NCAR reanalyses.

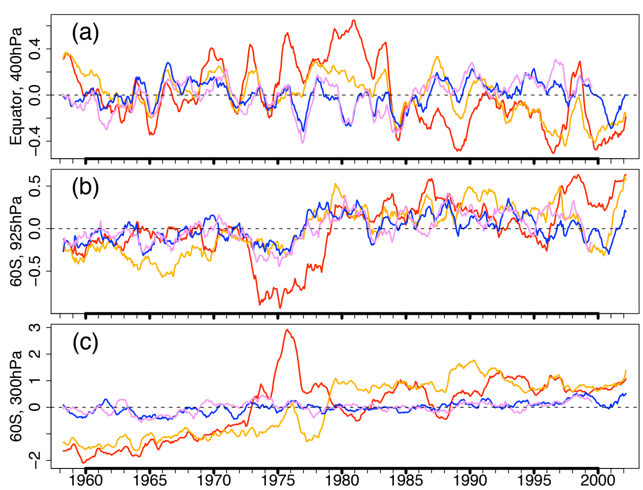

Figure 3. The one year running mean of zonally averaged air temperature residuals (a) at (Equator, 400 hPa) with TropSST filtering as described in the text; (b) at (60^0S,925hPa), without TropSST filtering ; (c) as in (b), at (60^0S,300hPa). ERA40 time series are shown in red, NCEP/NCAR in orange, HistSST in blue, and HistSST+AllForc in violet.